

The 3-Band Hubbard-Model versus the 1-Band Model for the high- T_c Cuprates: Pairing Dynamics, Superconductivity and the Ground-State Phase Diagram

W. Hanke¹, M.L. Kiesel¹, M. Aichhorn², S. Brehm¹, and E. Arrigoni³

¹ Institute for Theoretical Physics, University of Würzburg, Am Hubland, 97074 Würzburg, Germany

² Centre de Physique Théorique, École Polytechnique, CNRS, 91128 Palaiseau Cedex, France

³ Institute of Theoretical and Computational Physics, Graz University of Technology, Petersgasse 16, 8010 Graz, Austria

Abstract One central challenge in high- T_c superconductivity (SC) is to derive a detailed understanding for the specific role of the $Cu-d_{x^2-y^2}$ and $O-p_{x,y}$ orbital degrees of freedom. In most theoretical studies an effective one-band Hubbard (1BH) or t-J model has been used. Here, the physics is that of doping into a Mott-insulator, whereas the actual high- T_c cuprates are doped charge-transfer insulators. To shed light on the related question, where the material-dependent physics enters, we compare the competing magnetic and superconducting phases in the ground state, the single- and two-particle excitations and, in particular, the pairing interaction and its dynamics in the three-band Hubbard (3BH) and 1BH-models. Using a cluster embedding scheme, i.e. the variational cluster approach (VCA), we find which frequencies are relevant for pairing in the two models as a function of interaction strength and doping: in the 3BH-models the interaction in the low- to optimal-doping regime is dominated by retarded pairing due to low-energy spin fluctuations with surprisingly little influence of inter-band (p-d charge) fluctuations. On the other hand, in the 1BH-model, in addition a part comes from "high-energy" excited states (Hubbard band), which may be identified with a non-retarded contribution. We find these differences between a charge-transfer and a Mott insulator to be renormalized away for the ground-state phase diagram of the 3BH- and 1BH-models, which are in close overall agreement, i.e. are "universal". On the other hand, we expect the differences - and thus, the material dependence to show up in the "non-universal" finite-T phase diagram (T_c -values).

1) Introduction

Many aspects of the physics of high-temperature superconductors (HTSC) remain mysterious, despite impressive progress both on the experimental and theoretical front. One key issue, is why are the HTSC materials composed out of CuO_2 planes and what is the specific role of $Cu-d$ and $O-p$ orbital degrees of freedom? The cuprate materials in the undoped, i.e. "half-filled" situation, are "charge-transfer" insulators [1,2]. This fact induces an experimentally observed asymmetry between hole (h)- and electron (e)-doping: while doped holes go onto O orbitals and may be bound to Cu spins to form "Zhang-Rice" singlets, doped electrons reside mainly on the Cu orbitals [3,4,5,6,7,8,9,10]. This is believed to be intimately related to the more extended stability of antiferromagnetic (AF) behavior as a function of electron doping compared to that of hole doping. While introducing electrons on the Cu sites merely produces a dilution of spins, holes on O sites create a ferromagnetic coupling between neighboring Cu orbitals, which is significantly more effective in destroying the AF order. Beyond magnetism, the asymmetry is also exposed in the superconducting (SC) behavior with the h -doped materials exhibiting SC usually

over wide doping regimes and with high T_c 's up to 150K, whereas in the e -doped system T_c is low and confined to a very narrow doping regime.

In much of the high- T_c theoretical studies the starting point has not been the above three-band Hubbard (3BH) but instead the one-band Hubbard (1BH) and t - J models [11,3]. Here, the oxygen degrees of freedom are eliminated approximatively via the Zhang-Rice construction [3]. The mapping has as a crucial consequence that the undoped model systems are Mott insulators and no longer governed by the charge-transfer energy Δ_{pd} between the Cu and O orbitals. Analytical and, in particular, numerical calculations based on these two-dimensional (2D) single-band models have demonstrated Fermi surfaces, single-particle spectral weights, AF spin correlations and $d_{x^2-y^2}$ pairing correlations in qualitative agreement with experimental measurements [12,13,14,15,16,17,18,19,20]. This fact has significantly contributed to the wide-spread belief that the physics of HTSC is that of "doping into a Mott insulator" [21]. However, how can this picture be reconciled with the charge-transfer insulator picture embedded in the 3BH-model? Can it be that the charge-transfer energy Δ_{pd} in the 3BH-model, the size of which is already decisive for the accuracy of the 1-band reduction [3], plays the role of an effective on-site Hubbard U in the 1-band models?

Quantifying these ideas requires solving the strongly correlated electron problem for the 3BH- and 1BH-models at very low energy (and/or temperatures). Early Quantum-Monte-Carlo (QMC) calculations for the 3BH-model showed, that characteristic features such as the doping dependence of the electronic single-particle excitations and their interplay with magnetic excitations are in accord with experiment [4,5]. However, the very low T - or ground-state properties including the SC state, could not reliably be resolved, due to the well-known "minus-sign" problem [22]. Embedded cluster techniques provide a controlled way to approach the infinite-size (and, thereby, low-energy) limit. Recently, the variational cluster approach (VCA) which was proposed by M. Potthoff and our group [23,24] has been shown for the 1BH model to correctly reproduce salient features of the ground-state ($T = 0$) phase diagram of the high- T_c cuprates [14,16,17,25]. In particular, the AF and d-wave SC ground-states were found in doping ranges qualitatively in accord with experimental data for both e - and h -doping such as the different stability of the AF phase. It can be accounted for by a "simple" 1BH model, in which the e - h symmetry is broken by a longer-ranged (next-nearest) hopping term.

Regarding the possibility of the reduction to a one-band model, there are questions concerning the direct applicability of the Zhang-Rice (ZR) construction. As discussed in the literature before [9], the natural tendency of a finite oxygen band width is to delocalize and to destabilize the ZR singlets. Secondly, the pragmatic finding that a t - t' - U 1BH-model with a significant value of t' , captures basic physics of the cuprates and in particular their e - h asymmetry, cannot be accounted for in a strict ZR picture [26]. In this picture, next-nearest neighbor hoppings are very small compared to nearest-neighbor terms (if again oxygen-oxygen hopping t_{pp} is taken into account). What we will show in our calculations is that the 3BH-model and a single-band t - t' - U Hubbard model with a significant value for t' (which may be taken as an empirical parameter adjusted to fit the Fermi-surface topology [27]) exhibit a similar low-energy (here specifically, $T = 0$) physics concerning the qualitative behavior of the ground-state phase diagram [28] and of the single-particle excitations including the asymmetry as a function of h - and e - doping.

Then, where do the cuprate material-specific properties appear? To shed light on this question, we start out in section III with contrasting the low- T_c pairing mechanism with a discussion of what we know about the high- T_c mechanism. In particular, we take up an issue raised recently by P.W. Anderson [29], whether the pairing interaction in the cuprate HTSC should be considered as arising from a "pairing glue". Anderson argued that there is no room left for a pairing glue: while the low- T_c SC pairing is due to the well-known dynamic screening mechanism which contains a (phononic) "pairing glue", in the high- T_c cuprates and other unconventional SC another mechanism is at work. It may be termed "anisotropic real- or momentum-space" pairing. Here, the electrons pair in an anisotropic wave function (such as d-wave), which vanishes at the repulsive core of the Coulomb interaction. While this anisotropy is certainly realized for the cuprate HTSC and embedded in the momentum dependence of the d-wave gap function, there is, additionally, a frequency dependence of the SC gap, which tells us about the dynamics of the pairing interaction [30]. We study in section IV the dynamics of the SC gap function and the building up of a "pairing glue" which contributes to the formation of Cooper pairs in the 3BH-model and contrast it with the corresponding "pairing glue" for the 1BH-model. The "pairing glue" question is a natural one to ask if one has two-particle excitations, which are responsible for the dynamics of the pairing interaction, whose energy scale is small and of the order of the SC gap energy. For the 1-band models this "pairing glue"

issue has recently been investigated [30,31,32]. Spin fluctuations create a retarded interaction, which is dominating the low-energy pairing. However, also a pairing contribution due to interband (lower and upper Hubbard band) transitions was identified [30] in the 1BH-model case. In our calculation for the 1BH-model, this "non-retarded", i.e. spin-fluctuation dominated part is comparable in magnitude to a second part: For large U 's this creates an "instantaneous" pairing interaction eventually going over into the instantaneous part previously identified in the t - J model [30].

There are even qualitative differences in the dynamics of the pairing interaction in the 3BH-model: here, the dynamics of the pairing interaction is dominated by the retarded contribution due to spin fluctuations. Higher-energy p-d charge fluctuations give rise to a surprisingly small further (retarded) contribution. As expected, this charge-fluctuation contribution gains slightly more weight, when going to higher hole dopings. In short, one may term the dynamics of the pairing interaction in the 3BH-model and, thus, in a doped charge-transfer insulator as retarded and being due to a low-energy pairing glue, whereas in the 1BH-model and, thus, a doped Mott insulator both retarded and non-retarded parts contribute. The differences in the dynamics of the pairing interaction, which are due to the material dependent CuO_2 -physics, appear at relatively large energies (of order Δ_{pd}) which are significantly larger than the SC gap. In the ground-state phase diagram these "high-energy" differences are renormalized away (see, Fig. 5, in section IV). We do, however, expect that they play a role in the finite-T phase diagram (T_c -values).

Also the low-energy single-particle excitations of the 3BH- and 1BH-model are qualitatively similar, when comparing the 3BH-model with the (as discussed above) empirical t - t' - U model. A detailed discussion of this was presented in Ref. [25]. This concerns, in particular, where holes or electrons, respectively, go when one dopes away from half-filling. The corresponding nodal and anti-nodal doping regimes are directly related to the observed asymmetry in the robustness of the AF order. Closer inspection, however, also reveals differences for higher energies of $\mathcal{O}(t_{pd})$. An example is the recently much discussed "waterfall" structure or high-energy kink appearing as an abrupt change in the band dispersion, which falls vertically at binding energies below $\approx 0.4eV$ [33]. This "waterfall" behavior is found to be rather pronounced in the 3BH model, but not in the 1BH-model.

Finally, in section V, we describe a theory we have recently developed of two-particle (2-p) excitations and, in particular, the magnetic susceptibility in high- T_c cuprate superconductors [34]. As just discussed, 2-p excitations such as spin and charge excitations, play a key role in the pairing theory. There, they are indirectly embedded in the anomalous part of the selfenergy and the dynamics of the gap function. However, for an unambiguous identification, for example of a "pairing glue", one obviously needs a direct scheme for calculating these 2-p excitations in the experimentally relevant strong-correlation regime. Therefore, we have recently extended the Variational Cluster Approach to these excitations [34]. We found for the 1BH-model, that the corresponding magnetic susceptibility χ_s reproduces salient features of the experiment such as the celebrated neutron-scattering resonance in the hole-doped case. Previous descriptions of the magnetic resonance have been obtained by weak-coupling [35] and/or semiphenomenological approaches [36] and, quite independently, by the $SO(5)$ -symmetry argument [37]. The infinite-lattice limit is crucial to obtain the magnetic resonance which may be considered as a "fingerprint" of the AF order in the SC state. Only then are we able to differentiate between the competing AF and SC orders in the phase diagram. Therefore, this limit, which is obtained with the VCA, has also to be embedded in a controlled description of the corresponding susceptibilities.

In section V, we also study the emergence of a similar magnetic resonance in the SC state of the electron-doped cuprate superconductors. We find again for the 1BH-model case, that the experimentally observed resonance peak is consistent with an overdamped magnetic (spin $S=1$) exciton located near the particle-hole continuum. Because of computational reasons (reference cluster size) we can only demonstrate the magnetic resonance for the 1BH-model.

II) The Models

We consider the following version of the three-band Hubbard model:

$$\begin{aligned}
H = & \sum_{\sigma, \langle ij \rangle} t_{ij} \left(d_{i\sigma}^\dagger p_{j\sigma} + H.c. \right) + \sum_{\sigma, \langle jj' \rangle} \bar{t}_{jj'} \left(p_{j\sigma}^\dagger p_{j'\sigma} + H.c. \right) + (\epsilon_d - \mu) \sum_{\sigma, i} n_{i\sigma}^d \\
& + (\epsilon_d - \mu) \sum_{\sigma, j} n_{j\sigma}^p + U_{dd} \sum_i n_{i\uparrow}^d n_{i\downarrow}^d + U_{pp} \sum_i n_{i\uparrow}^p n_{i\downarrow}^p + U_{pd} \sum_{\sigma\sigma', \langle ij \rangle} n_{i\sigma}^d n_{j\sigma'}^p
\end{aligned} \tag{1}$$

where $d_{j\sigma}^\dagger$ creates a hole with spin σ in the $Cu-d_{x^2-y^2}$ orbital at site i with occupation number $n_{i\sigma}^d$. Correspondingly, $p_{j\sigma}^\dagger$ creates an $O-p_{x,y}$ hole at site j with occupation number $n_{j\sigma}^p$. t_{ij} stands for the p-d hybridization t_{Cu-O} and $\bar{t}_{jj'}$ for the direct $O-O$ hopping, where the orbital phase factors are included [4,5]. The local orbital levels are given by ϵ_p and ϵ_d and the charge-transfer energy is $\Delta = \epsilon_p - \epsilon_d$. U_{dd} and U_{pp} are the Hubbard couplings on the Cu and O sites, respectively. Finally, U_{pd} is a repulsive interaction for holes on Cu and O . We take typical parameters consistent with earlier extensive Quantum-Monte-Carlo (QMC) [4,5] as well as cluster [27] calculations. In units of the $Cu-O$ hopping $t_{pd} = 1$, $\Delta = 3$, $U_{dd} = 8$, $U_{pd} = 0.5$, $U_{pp} = 3.5$ and $t_{pp} = 0.5$.

The 1BH-model is defined as usual, i.e.

$$H = \sum_{\sigma, \langle ij \rangle} t_{ij} c_{i\sigma}^\dagger c_{j\sigma} + U \sum_i n_{i\uparrow} n_{i\downarrow}. \tag{2}$$

Here $c_{j\sigma}$ and $c_{i\sigma}^\dagger$ are annihilation and creation operators and t_{ij} denote the nearest ($t_{nn} = 1$, energy unit) and next-nearest neighbor ($t_{nnn} = -0.3$) hopping matrix elements and U ($U = 8$) the on-site Hubbard repulsion.

An important remark for the comparison of the two models is that while for the 3BH-model the unit is $t_{pd} = 1$ and $t_{nn} = t = 1$ for the 1BH-model, when going back to eV's one has to set $t_{pd} \cong 1.5[eV]$ and $t \cong 0.4[eV]$.

III) Low- T_c versus high- T_c superconductivity and the question of the pairing glue.

In a recent article [29], P. W. Anderson (PWA) has argued that pairing in conventional ‘‘low- T_c ’’ superconductors (SC) has a rather different microscopic origin from that in high- T_c cuprates and many other unconventional SC. In either case, the paired electrons have to avoid the strongly repulsive bare Coulomb interaction.

In a *low- T_c SC* this repulsion can be eliminated in favor of electron-pair binding via ‘‘dynamic screening’’, i. e.

$$V(\mathbf{q}, \omega) = \frac{e^2}{q^2 \varepsilon(\mathbf{q}, \omega)}, \tag{3}$$

where $V(\mathbf{q}, \omega)$ is the Fourier transform of the el-el interaction in both space and time and $\varepsilon(\mathbf{q}, \omega)$ is the dynamic screening due to both ions and electrons, i.e. $\varepsilon(\mathbf{q}, \omega) = \varepsilon_{ion}(\mathbf{q}, \omega) + \varepsilon_{el}(\mathbf{q}, \omega)$.

PWA then gives an elegant discussion why, in his opinion, in the *high- T_c SC* another pairing mechanism is at work, which may be termed ‘‘anisotropic momentum (or real-space) mechanism’’: here, the strongly repulsive (short-range) part of the Coulomb interaction is avoided by a mechanism suggested by Pitaevskii [38] and Brueckner et. al. [39] of choosing the pair state orthogonal to the repulsive core of the Coulomb interaction, i.e. putting the electron pairs in an anisotropic wave function (such as d-wave), which vanishes at the core of the Coulomb interaction.

While we follow the arguments of PWA for the low- T_c SC, we would like to present here evidence, that *in the high- T_c materials both the anisotropic ‘‘momentum space’’ mechanism and the dynamics* are

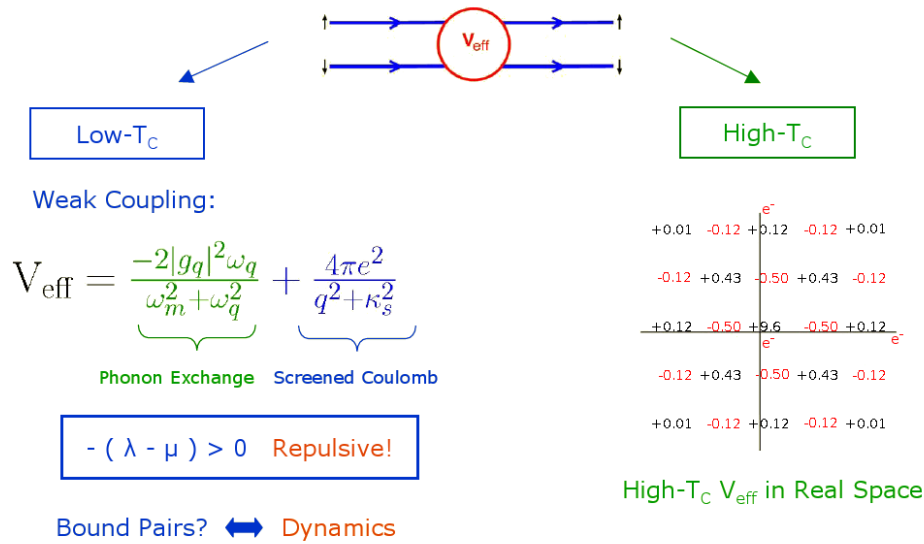


Figure 1. The effective pairing interaction in the weak-coupling low- T_c situation compared with high- T_c QMC simulations for the 2D 1-band Hubbard model by the Scalapino group [43].

at work. In what follows this will be shown for both of the above Hubbard-type of models (see chapter IV). This gives us, in particular, a possibility to shed light on the question to what extent both models lead to a similar pairing mechanism. For the 1-band Hubbard model, the reader is also referred to recent studies by Maier, Poilblanc and Scalapino [30] as well as by Kyung, Sênèchal and Tremblay [31], where also the pairing dynamics has been studied. The above questions are clearly of relevance for the main issue raised by PWA, namely “is there glue in cuprate superconductors?”, which is basically a question about the dynamics of the pairing interaction. As argued by Maier et al., if the dynamics of the pairing interaction arises from virtual states, whose energies correspond to the “high-energy” Mott gap, and give rise to the exchange coupling J , the *interaction is instantaneous on the relative time scales of interest*. However, if the energies correspond to typical “low-energy” spin-fluctuation (or phonon) excitations, then the *interaction is retarded*. In this case it makes sense to use the terminology “spin-fluctuation glue”, which mediates the d-wave pairing. Here, we present results from numerical (variational cluster) studies, which provide insight into this question.

For this presentation it is useful to step by step *contrast* the construction of the *effective el-el interaction for a weak-coupling low- T_c SC with the effective interaction of a high- T_c (i.e. Hubbard type) SC*. In the “dynamic screening” mechanism of eq. (3) one can safely replace the electronic screening by a static one (i.e. $\varepsilon_{el}(\mathbf{q}, \omega = 0)$). This is due to the fact that typical el-energies are of “high energy” ($\sim \mathcal{O}(\varepsilon_{Fermi})$) compared to $k_B T_c$, i.e. the SC energy scale: the plasma of other electrons then damps away the long-range ($1/r$)-behavior and leaves a Thomas-Fermi screened core $e^2 e^{-x r} / r$ (x : Thomas-Fermi constant). This gives rise to an essentially instantaneous interaction, which is still “very repulsive”, and which - when averaged over the Fermi surface - is termed μ (see below). On the other hand, for the phonon case, the screening acts anti-adiabatically, i.e. $\varepsilon_{ion}(\mathbf{q}, \omega)$ is dynamic, since typical phonon frequencies are of the order of $k_B T_c$. In other words, the final Fourier-transformed effective interaction is $V_{\text{eff}} = \frac{e^2}{[(q^2 + x^2)\varepsilon(q, \omega)]}$, and the effective electronic interaction is screened (anti-adiabatically) by the phonon polarizations.

Fig. 1 summarizes this weak-coupling low- T_c situation and rewrites the effective pairing interaction as the usual sum of the dynamic phonon exchange and the Thomas-Fermi screened Coulomb part. Here ω_q denotes phonon (ph) frequencies, $g_{\mathbf{q}}$ the el-ph coupling and ω_m are Matsubara frequencies. When the two terms in the sum are averaged over the Fermi surface (the brackets in Fig. 2 for V_{eff} denote an average of the momentum transfer q over ε_F), then one finds that the corresponding averaged V_{eff} is larger than zero, i.e. $-(\lambda - \mu) > 0$ and, thus, is still repulsive. The net interaction is thus repulsive even in the phonon case, a fact which is required to guarantee the stability of the solid.

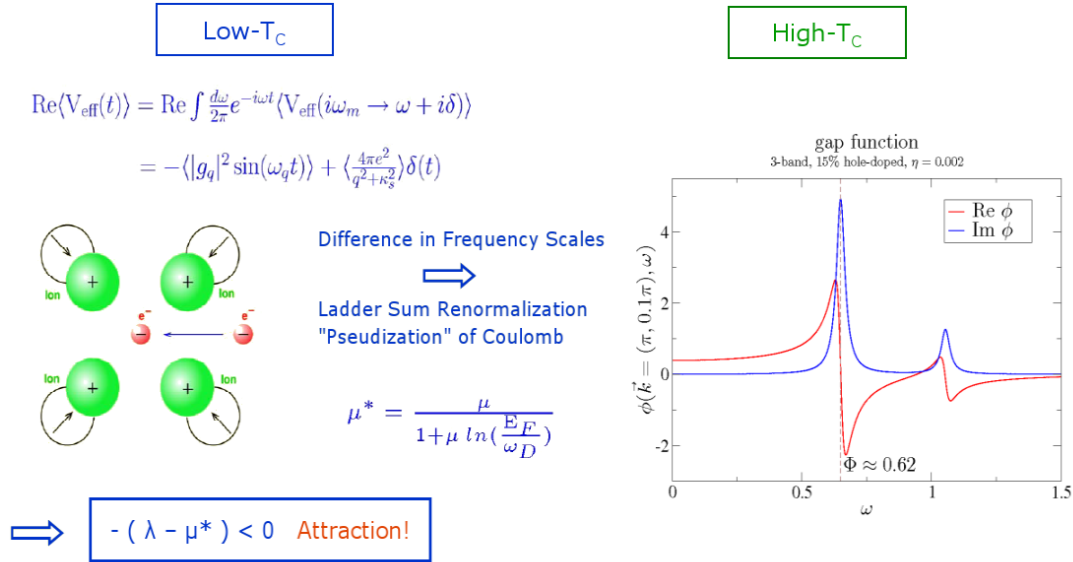


Figure 2. left-hand part: Dynamics of the pairing interaction for the low- T_c case: the emergence of the difference in frequency scales, i.e. slow ionic-lattice polarization and fast Coulomb repulsion. Right-hand part: the SC gap function and its dynamics (both Re- and Im- parts) for the 3BH-model. Note that the Re-part displays a certain similarity to the gap function shown for the low- T_c case in the left-hand part of Fig. 3. This is true for the spin-fluctuation contribution appearing around the characteristic energy $\omega_0 + \Delta_0 \cong \Phi$ (see also Fig. 6f)). At higher energies of order $\omega \cong 1$ and above additional structure appears mainly due to $p-d$ charge fluctuations (see again Fig. 6f)).

So, how can one ever arrive at bound pairs, if the interaction is never attractive? As is well-known since Cooper's seminal paper [40] preceding BCS-theory, this is due to the difference in frequency scales or, equivalently, in time scales of the two parts of the interaction. This is pictured in Fig. 2: the "first" electron (anti-adiabatically) polarizes the ionic lattice and sets up a net negative charge polarization in its vicinity. This first process is "slow" and happens on the frequency scale ω_q of the ionic vibrations. A "second" electron feels this polarization, but can only profit from it and build up an effective attraction when the first electron "instantaneously" moves so as to avoid each other. Thus, the "high-energy" part of the Coulomb interaction acts only over a short time, given here by a δ -function, while the attractive el-ph interaction is *retarded* by the much slower lattice response. In other words, if the electrons forming the pair correlate themselves in time to avoid the short-time Coulomb repulsion, they can take advantage of the attractive el-ph mediated interaction and form a Cooper pair. As is well-known, this kind of renormalization, i. e. integrating out the "high-energy" degrees of freedom in the relative pair wave function (so that one arrives at one and the same low-energy cutoff of order of the Debye frequency ω_D in Fig. 2), can be done a variety of ways: by a ladder sum renormalization or a "pseudization" of the interaction, replacing μ by μ^* [41]. Now, we can have $-(\lambda - \mu^*) < 0$, i.e. a situation where V_{eff} can be attractive, leading in Cooper's sense to the pairing instability at very low energies.

We are interested in the dynamics of the pairing interaction in the *high- T_c cuprates* and, in particular, how there the two electrons about to form a pair can avoid each other - and thus weaken their repulsion - by modifying the high-energy parts of their relative wave function. For this, it is instructive to look first at the frequency dependence of the gap function of a low- T_c SC found by solving the Eliashberg equations [42], following a discussion by D. J. Scalapino [43] (see the low- T_c case in Fig. 3): The real part of the corresponding gap function $\Delta(\omega)$ first increases as the typical phonon energy ω_q is approached. At this characteristic "glue energy", it changes sign and remains negative out to very large values of ω . This latter observation corresponds to the instantaneous part. It just reflects the fact that the two electrons making up the pair avoid "short-time close-range encounters". This can be summarized (see Fig. 3) in a kind of orthogonality relation, with the pair wave function $\Delta(\omega)$ being orthogonal to the "core" (i.e. the Thomas-Fermi screened short-range part) of the Coulomb interaction [43]. The essence of this orthogonality relation is that in practice $\langle 4\pi e^2 / (q^2 + x^2) \rangle$ can be replaced over the frequency integral Δ to several times the Debye frequency ω_D by the weak pseudopotential μ^* [41] [43].

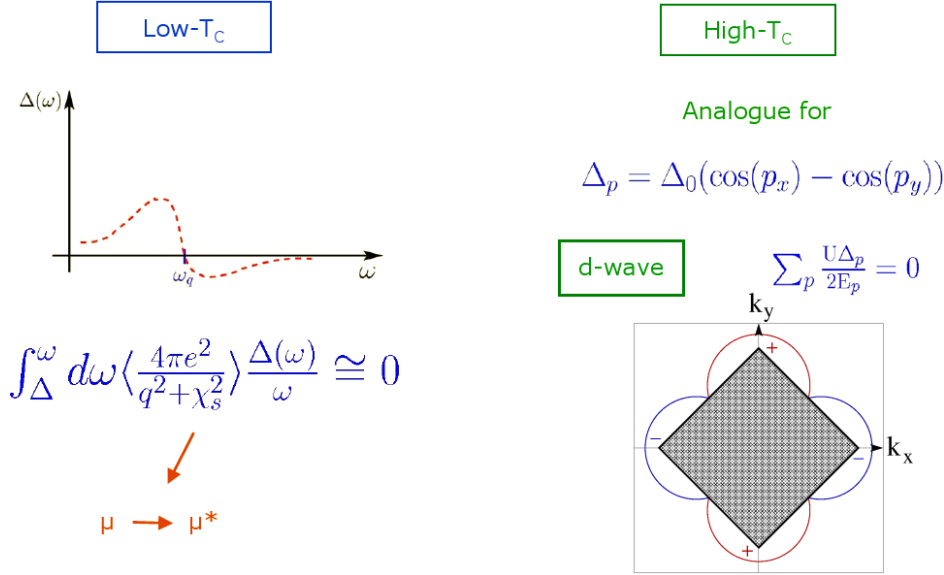


Figure 3. Avoiding the strongly repulsive part of the Coulomb repulsion: Analogy of the gap function Δ in the low- T_c (ω -space) and high- T_c (momentum-space) situation. The figure for the momentum-space gap function in the high- T_c -case is again taken from [43]. Here, the shaded region is the normal-state Fermi surface and the solid curve surrounding the Fermi surface gives the size of the $d_{x^2-y^2}$ -gap Δ_k at the momentum k on this surface.

So then, how do the electrons in high- T_c materials act so that they are seldom or never in the same place at the same time?

Here, it is useful to first look at the effective interaction V_{eff} in real-space (or, more precisely, at the real-space Fourier transform of the singlet vertex $\Gamma(l, \omega_m = 0)$ [42] versus the separation l between the electrons in pairs). Figs. 1 & 3 plot the results for V_{eff} obtained from QMC simulations for the 2D 1-band Hubbard model by the Scalapino group [43]. We have obtained a similar pattern for the effective interaction in the 3BH-model employing also QMC, when again the two electrons are placed on the Cu-lattice sites [44].

Using the BCS gap equation for illustration, i.e.

$$\Delta_p = - \sum_{p'} V_{pp'} \frac{\Delta_{p'}}{2E_{p'}}, \quad (4)$$

with $V_{pp'}$, the effective interaction or Fourier-transformed vertex $V_{pp'} = T(p' - p)$, we immediately see that the two pairing electrons avoid the repulsive parts of the Coulomb interaction by arranging their pair wave-function in a $d_{x^2-y^2}$ -orbit, with the simplest nearest-neighbor pairing given in momentum space by $\Delta_p = \Delta_0(\cos p_x - \cos p_y)$. This is expressed by a kind of Pitaevskii-Brueckner relation, i.e.

$$\sum_{p'} \frac{U \Delta'_p}{2E'_p} = 0, \quad (5)$$

This latter relation indeed seems to confirm PWA's conjecture in that the essence of the pairing mechanism in low- T_c SC is "dynamic screening", whereas in the high- T_c cuprates it is "anisotropic momentum space pairing". In Fig. 2, we see - however - that the dynamics of the pairing interaction as reflected in the ω -dependence of the gap function $\Delta(\omega)$, is also of relevance for the high- T_c cuprates. Here again, the real part of the gap function changes sign at a characteristic frequency Φ related to spin fluctuations and at higher energies to $p-d$ charge fluctuations.

IV) Dynamics of the pairing interaction in the 1BH- and 3BH-models

The question of whether one can speak of a “pairing glue” has recently been addressed by Maier, Poilblanc and Scalapino for the 1BH- and t - J models [30]. If the dynamics of the pairing interaction is due to “small-energy” (two-particle) excitations, such as the characteristic structures seen in the spin susceptibility, then one might speak of the interaction as being retarded on the relative time scales of interest and of a “spin-fluctuation” glue mediating d-wave pairing. This clearly is reminiscent of the usual phonon mediated pairing interaction in the low- T_c SC [30].

It is well-known that for these latter systems the gap function $\phi(\mathbf{k}, \omega)$ or, more precisely, the anomalous part of the Nambu selfenergy $\Sigma(\mathbf{k}; \omega)$, is only very weakly depending on momentum \mathbf{k} , corresponding to the local character of the pairing interaction. However, the dynamics of the gap function is important and it enters the dispersion (Cauchy) relations between the real and imaginary parts of $\phi(\mathbf{k}, \omega) = \phi_1(\mathbf{k}, \omega) + i\phi_2(\mathbf{k}, \omega)$, i.e.

$$\phi_1(\mathbf{k}, \omega) = \frac{1}{\pi} \int \frac{\phi_2(\mathbf{k}, \omega')}{\omega' - \omega} d\omega' \quad (6)$$

and, for $\omega = 0$,

$$\phi_1(\mathbf{k}, \omega = 0) = \frac{2}{\pi} \int \frac{\phi_2(\mathbf{k}, \omega')}{\omega'} d\omega' \quad (7)$$

A measure for the fractional contribution to the gap function $\phi(\mathbf{k}, \omega = 0)$ and to pairing that comes from frequencies less than Ω can then be defined [30], i.e.

$$I(\mathbf{k}, \Omega) = \frac{2}{\pi} \frac{\int_0^\Omega \frac{\phi_2(\mathbf{k}, \omega')}{\omega'} d\omega'}{\phi_1(\mathbf{k}, 0)} \quad (8)$$

It gives the relative contribution to the pairing of the retarded “glue” part and of the non-retarded, i.e. “instantaneous” part. In Ref [30] it has been demonstrated that $I(\mathbf{k}, \Omega)$ is a useful diagnostic for the pairing glue (phonon contributions) in the case of Pb . $I(\mathbf{k}, \Omega)$ increases as Ω passes through $\omega_{Phonon} + \Delta_0$, where Δ_0 denotes the SC gap and ω_0 the characteristic Pb phonon frequencies. Its asymptotic value $I(\mathbf{k}, \Omega \gg \omega_{Phonon} + \Delta_0)$ exceeds unity reflecting the fact there exists an instantaneous Coulomb pseudo-potential. This leads to a negative, frequency-independent contribution ϕ_{NR} to $\phi(\mathbf{k}, \omega)$ and at high frequencies $I(\mathbf{k}, \Omega)$ exceeds 1 by the “instantaneous” contribution $-\phi_{NR}/\phi_{(0)}$. Here, using numerical techniques, we examine the question of a “pairing glue” which offers a way of distinguishing different pairing mechanisms for the one-band and three-band Hubbard models in the relevant strong-correlation regime for the HTSC.

The variational cluster approach (VCA) is particularly well suited for a study of the quantity $I(\mathbf{k}, \Omega)$. This is due to the fact that the VCA allows for accurately calculating the real and imaginary parts of the anomalous self-energy and, thus, of the gap function $\phi_1(\mathbf{k}, \omega)$. This has already been shown in a recent letter, reproducing the experimentally found “gap dichotomy” of the nodal and anti-nodal gaps in HTSC as a function of doping [17].

In the VCA for the Hubbard model, the lattice is tiled up with (isolated) clusters of a given size. The corresponding Hamiltonian H' has the same on-site interaction U as the original Hubbard model, but it has modified single-particle hopping parameters t' (and chemical potential μ') with, in particular, $t' = 0$ between different clusters. The cluster provides a “reference system”, which spans a space of trial self-energies $\Sigma(H')$. The self-energy that “best” describes the physics of the infinite lattice is then constructed via a variational principle, searching for the stationarity of the ground potential $\Omega(\Sigma)$ in the subspace of the cluster self-energies $\Sigma(H')$. The trial self-energies $\Sigma(H')$ are varied by varying the parameters t' , μ'

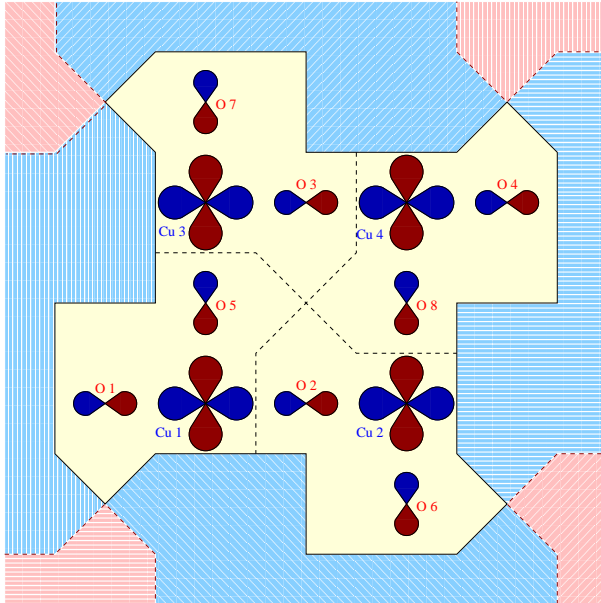


Figure 4. (2×2) reference cluster used for 3BH-model. Each cell contains a CuO_2 unit. To reduce finite-size effects in 2-particle correlations, a more symmetric arrangement of O sites is implemented, compared to previous publications (see Ref. [25]).

and the Weiss (i.e. pairing, AF, etc.) fields and a local chemical potential-shift term, which guarantees a consistent treatment of the particle density [24]. For the SC ground-state, a Nambu representation of the self-energy is used and $\phi(\mathbf{k}, \omega)$ is obtained from the τ_1 -component.

The results for $I(\mathbf{k}, \Omega)$ for the 3BH-model to be discussed below, are based on a (2×2) cluster with 4 CuO_2 unit-cells and the self-energy (and Green's function) of this 12-site cluster was extracted from exact diagonalization. The geometry of our reference cluster is reproduced in Fig. 4. As we found 2-particle correlation functions on a small cluster to be more sensitive to symmetry than the 1-particle spectral functions and the phase diagram, we use a symmetric arrangement of the O sites in the reference cluster. Additionally, the Coulomb interaction U_{pd} between holes on Cu and O sites is implemented with periodic boundary conditions.

On the other hand, the results for the 3BH-model phase diagram in Figs. 5 and the 1-particle excitations in Figs. 6 a) & d) are in close agreement with our earlier results published in Ref. [25], where we used a (not-symmetrized) (2×2) cluster. The “upshot” of these results is, that the 3BH- and the 1BH-model phase diagram results with the latter presented in Figs. 5 a) & c) are very similar, reproducing in both cases the overall ground-state phase diagram of the high- T_c superconductors (see also Fig. 3 of Ref. [25]). In particular, they include salient features, such as the enhanced robustness of the AF state as a function of electron doping and the tendency towards phase separation (“PS” regime) into a mixed AF-SC phase at low doping and a pure SC phase at high (both hole and electron) doping. In the low-doping regimes, we find at a homogeneous symmetry-broken state in which both, the AF and the d-wave SC order parameters m and Δ are nonzero. This corresponds to a phase “AF+SC”, where AF and d-wave SC order microscopically coexist. A homogeneous state with pure d-wave SC ($m = 0$ and $\Delta > 0$) is obtained in the larger doping regimes. In the “in between doping” regions macroscopic phase separation occurs, where these two latter phases are thermodynamically unstable. In previous work, we have shown for the 1BH-model, that larger reference clusters still yield a qualitatively similar phase diagram, with one notable exception: the larger clusters (up to 10 sites in the 1BH-model) results suggest, that phase separation remains persistent in the h-doped case and disappears in the e -doped situation [28]. Based on the overall very similar phase diagrams for the (2×2) 3BH-model and for the (4×2) 1BH-model (Figs. 5 b) & d)), we expect a similar disappearance of the “PS”-region for e -doping also in the 3BH-model.

Why are the phase diagrams in Fig. 5 so similar despite the fact that, for example, the p-d charge fluctuations give rise to an at higher energies ($\omega \sim \Delta_{pd}$) even qualitatively different behavior of the dynamic pairing interaction for the 3BH results when compared to the 1BH-data as shown in Figs. 6 & 7

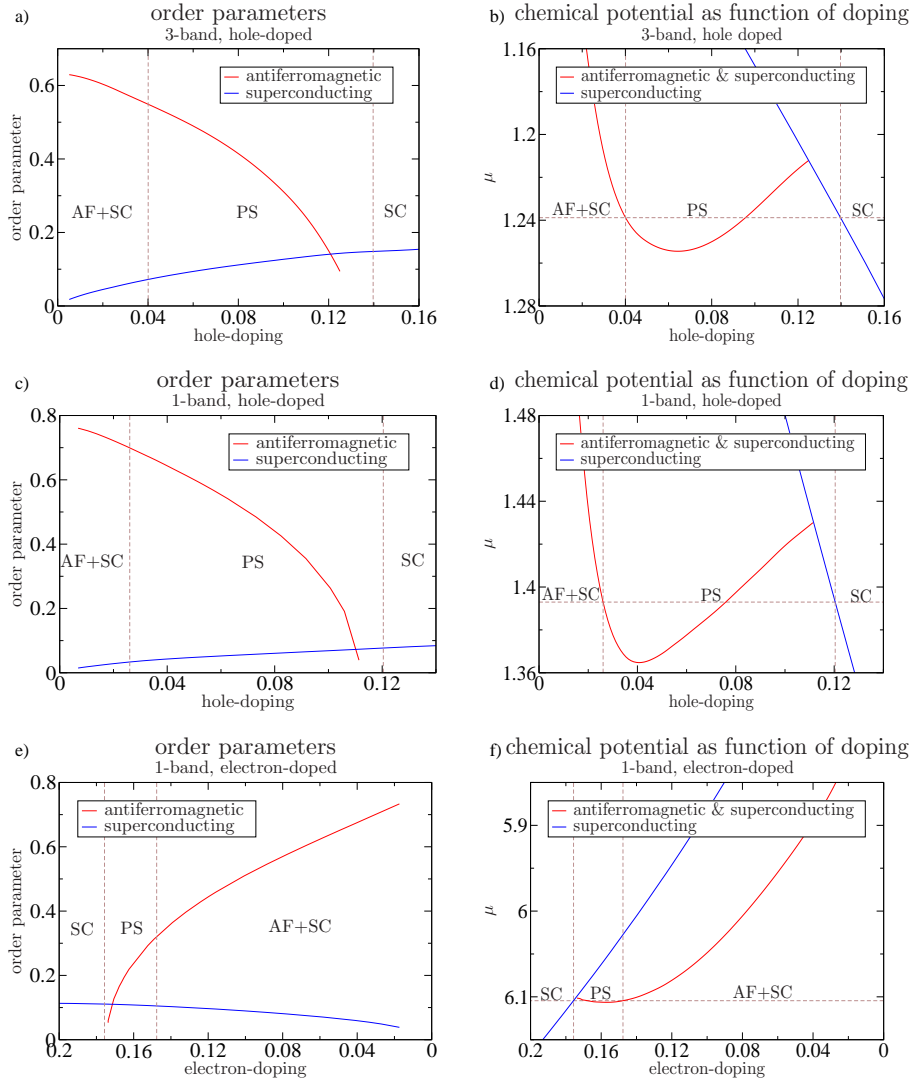


Figure 5. Ground-state phase diagram for the 3BH-model (a) & b), based on a (2×2) reference cluster with the parameters specified in the text, in comparison with the 1BH-model (c) - f), based on a (4×2) reference cluster. In d), e) & f), the chemical potential μ is plotted as a function of doping. The corresponding order parameters for the models are given in (a), c) & e)). Between the mixed phase with both antiferromagnetic and superconducting order (AF+SC) and the pure superconducting phase (SC) at higher-dopings, is a region of phase separation (PS), described in text. For 1BH-model, both hole- and electron-doping is presented. There is no qualitative difference between 1BH and 3BH phase diagrams.

for $I(\mathbf{k}, \Omega)$? The reason is that on the scale of the (maximal) d-wave gap energies, Δ_{pd} is a doping-independent “high-energy” scale (\sim ten times larger than the SC gap) the role of which is taken over in the 1BH-model by another doping independent “high-energy” scale, namely an effective Hubbard U (see discussions, below). As just stressed, however, the dynamics of the pairing mechanism, may be quite different, which is what we find indeed below. We expect this to be of importance for the “non-universality”, i.e. material-dependence of the cuprate SC.

Also the single-particle excitations (as displayed in Figs. 6 up to 7 as well as in our earlier Ref. [25]) are found qualitatively to be similar, concerning the “low-energy” physics and, in particular, the e - h asymmetry. This asymmetry explains the corresponding e - h asymmetry found in the ground-state phase diagram for the robustness of the AF phase (Figs. 5 c) & e): doped holes first enter around the nodal point $(\frac{\pi}{2}, \frac{\pi}{2})$, where the SC gap vanishes, introducing a “gap-less” screening which very effectively destroys long-range AF order [16]. In contrast, introducing electrons around the anti-nodal point $(\pi, 0)$ fixes μ (due to the large density of states) within the SC gap, in a regime where this gap is maximal.

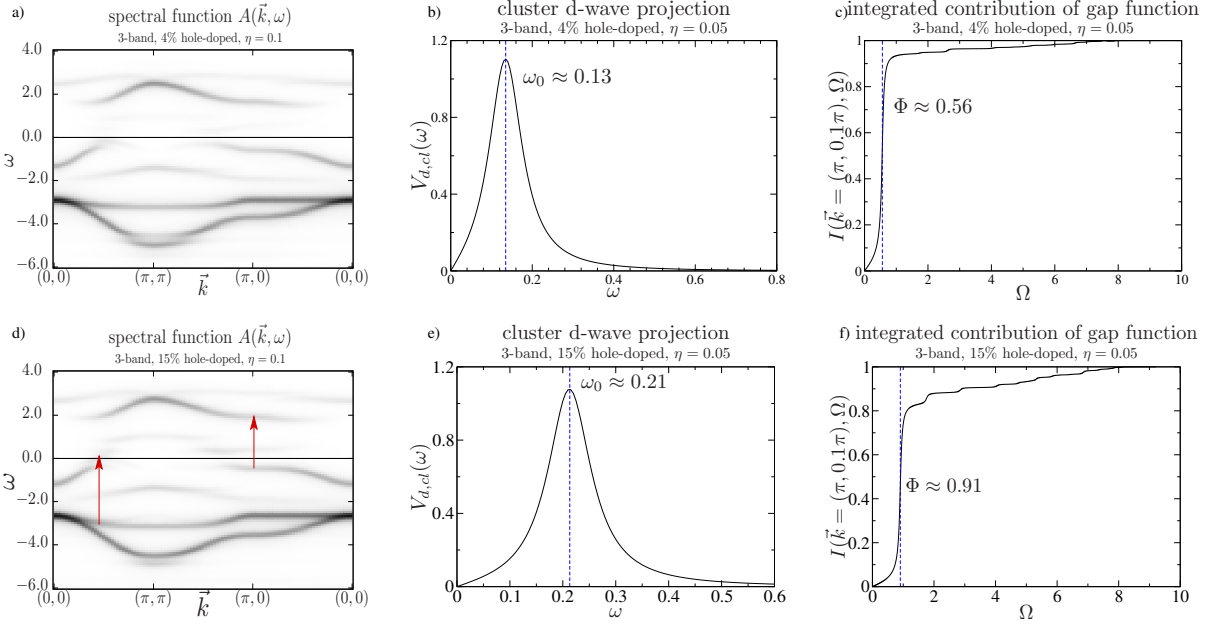


Figure 6. 3BH-model: single-particle spectral function $A(\mathbf{k}, \omega)$ (a) & d), d-wave projection $V_d(\omega)$ of the spin susceptibility (b) & e), see eq. (10) and integrated contribution of gap function $I(\mathbf{k} = (\pi, 0.1\pi), \Omega)$ (c) & f) for a (2×2) reference cluster (as in Fig. 4). For a) - c), the hole-doping is 4% and for d) - f), the hole-doping is 15%. For both dopings, the system is in a pure superconducting state.

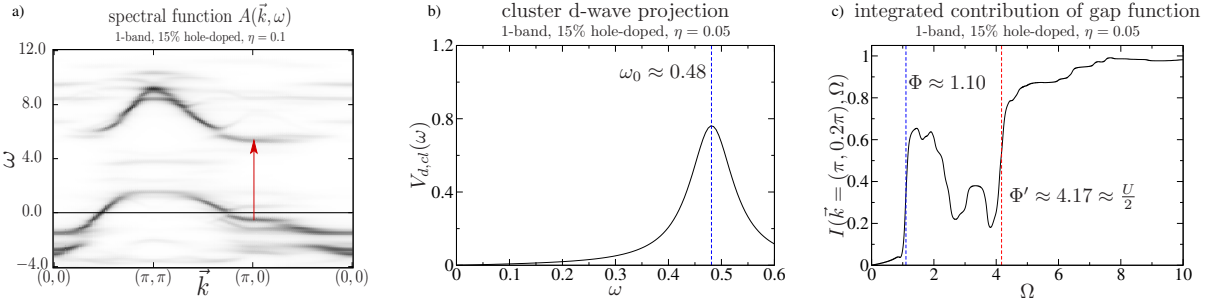


Figure 7. 1BH-model: single-particle spectral function $A(\mathbf{k}, \omega)$ (a), d-wave projection $V_d(\omega)$ of the spin susceptibility (b), see eq. (10) and integrated contribution of gap function $I(\mathbf{k} = (\pi, 0.2\pi), \Omega)$ (c) with a (3×3) reference cluster. Hole-doping is 15% and the system is in a pure superconducting state (see Fig. 6).

Here, an incomplete screening cannot disrupt AF order up to significantly large e -dopings where, finally, μ enters also here the “gap-less” $(\frac{\pi}{2}, \frac{\pi}{2})$ region. So again, it is the corresponding low-energy physics embedded in the qualitatively rather similar single-particle spectra plotted in Figs. 6 - 7, which determines salient (here AF) features of the phase diagram.

So, let us finally come back to the question of the dynamics in the pairing interaction and the fractional contribution $I(\mathbf{k}, \Omega)$ to the gap function in the 3BH- as well as 1BH- models.

Our results for $I(\mathbf{k}, \Omega)$ for the 3BH-model, i.e. for the fraction of the zero-frequency gap function which arises from frequencies below Ω , are plotted in Figs. 6 c) & f). Here two doping cases, 4% hole doping and 15% hole doping are shown, together with the corresponding single-particle spectral function $A(\mathbf{k}, \omega)$ and the data for the d-wave projection of the cluster spin susceptibility (eq. (10)).

$I(\mathbf{k}, \Omega)$ is plotted for the 3BH-model for a doping $x = 4\%$ in Fig. 6 c) and for a higher doping $x = 15\%$ in Fig. 6 f). $\mathbf{k} = \pi(0.1, 0)$, i. e. a \mathbf{k} -point close to the anti-nodal point $(\pi, 0)$ where the d-wave SC gap is maximal. For both dopings, we observe a first steep rise at a typical energy Φ of about $\omega_0 + \Delta_0$, where Δ_0 denotes the quasi-particle (SC) gap and ω_0 a characteristic spin-fluctuation frequency. Close to half-

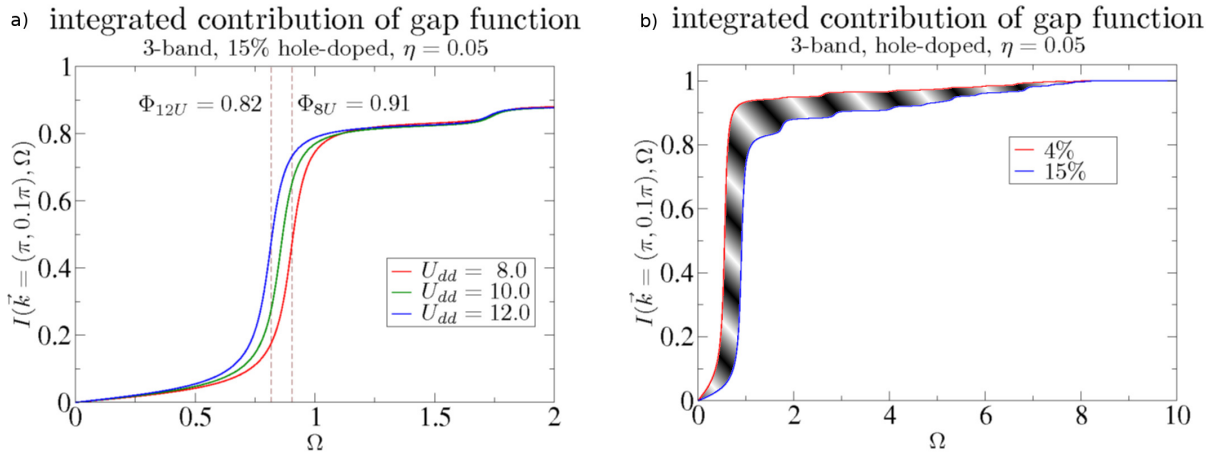


Figure 8. Integrated contribution of gap function $I(\mathbf{k} = (\pi, 0, 1\pi), \Omega)$ for the 3BH model. In a), the first dominant increase in $I(\mathbf{k}, \Omega)$ is plotted for different values of U_{dd}/t . In b), the doping dependence of $I(\mathbf{k}, \Omega)$ is shown, with the modest increase of p-d charge fluctuations as function of doping.

filling, ω_0 is roughly estimated by the strong-coupling result for the Cu - Cu exchange energy $\omega_0 \cong 2J_{Cu}$, with

$$J_{Cu} = \frac{4t_{pd}^4}{(\Delta_{pd} + U_{pd})^2} \left(\frac{1}{\Delta_{pd} + U_{pp}/2} + \frac{1}{U_{dd}} \right) \cong 0.1t_{pd}. \quad (9)$$

As shown by the d-wave projected result $V_{d,cl}(\omega)$ in Fig. 6 b) & e), for the imaginary part of the cluster spin susceptibility, with the definition

$$V_{d,cl}(\omega) = \frac{1}{N^2} \sum_{\mathbf{k}, \mathbf{k}'} (\cos(k_x) - \cos(k_y)) (\cos(k'_x) - \cos(k'_y)) \text{Im}\chi_{cl}(\mathbf{k} - \mathbf{k}', \omega), \quad (10)$$

the first dominant peak is found at low doping, i.e. 4% at about this energy (here $\omega_0 \cong 0.13$ as always in units of the hopping t_{pd}) and, at 15% doping at a higher energy $\omega_0 \cong 0.2$.

$I(\mathbf{k}, \Omega)$ displays an amazingly prominent first increase at an energy Φ of about $\Delta_0 + \omega_0$, where Δ_0 is the quasiparticle gap and ω_0 the first dominant peak in the d-wave projection of the dynamic spin susceptibility $\text{Im}\chi(\mathbf{k}, \omega)$. The quasiparticle gap is found to be at $\Delta_0 \cong 0.52$ (obtained from the spectral function) for 4% doping and at a similar value ($\Delta_0 \cong 0.41$) for 15% doping, thus $\Delta_0 + \omega_0 \cong 0.65$. The first sharp rise in $I(\mathbf{k}, \Omega)$ at the low-doping situation ($\sim 4\%$) is at about $\Phi \cong 0.56$. We observe that in this low-doping case for the 3BH-model more than 90% of the saturation value of $I(\mathbf{k}, \Omega) = 1$ is due to the dynamic contribution of the spin fluctuations.

For 15% doping ω_0 is increasing [13], and so is $\omega_0 + \Delta_0$. Fig. 8 a) further confirms the leading role of the spin-fluctuations. Here the first dominant increase in $I(\mathbf{k}, \Omega)$ is plotted as a function of U/t at 15% h-doping. One sees that as the value of U/t increases, this dominant increase in $I(\mathbf{k}, \Omega)$ is shifted to lower energies, scaling essentially with the exchange energy J (Δ_0 is found to be essentially constant as function of U/t). Here, at 15% doping, the spin-fluctuation contribution to the saturation value of $I(\mathbf{k}, \Omega) = 1$ slightly decreases compared to the 4%-doping situation. From there on a mild rise takes place, starting at about $\omega \cong 1$ for both dopings. In both doping cases this corresponds to virtual e-h transitions involving the charge transfer gap $\sim \Delta_{pd}/2$ (see Fig. 7a).

Fig. 8 b) illustrates the influence of the doping dependence of p-d charge fluctuations on $I(\mathbf{k}, \Omega)$. Here, at first glance, the influence of these fluctuations on the integrated gap function $I(\mathbf{k}, \Omega)$ appears to be very mild.

However, this picture changes significantly, when we confront the 3BH-model results for $I(\mathbf{k}, \Omega)$ in Figs. 6 d) - f) with the corresponding ones for the 1BH-model and, thus, the doped Mott-insulator case (Figs. 7 a) - c): again, we find for the latter model a first dominant rise in the integrated gap function. (We plot here only the results for the 15%-doping case with the low-doping (4%) results being qualitatively similar.) This first rise - when analyzing its (U/t) -dependence - can again be attributed to dynamic spin excitations. However, a second prominent increase in this 1BH-model case occurs after a rather pronounced drop at energies of order $(U/t)/2$. This has already been observed in this 1BH-model case in Ref. [30] and was termed a “non-retarded” contribution occurring at an energy scale set by the Mott gap and being related to excited states (see the red arrow in the corresponding $A(\mathbf{k}, \omega)$ spectrum in Fig. 7 a) involving the upper Hubbard band. For the t - J model, Ref [30] finds this energy scale being pushed to “infinity”, with the corresponding exchange interaction being instantaneous. In contrast, the retarded (spin-fluctuation) interaction, i.e. the first steep rise in $I(\mathbf{k}, \Omega)$, occurs at an energy scale which is small ($\omega_0 \cong 0.1t$) compared to the bare bandwidth $8t$ (and the bare U). Thus, the *1BH-model as well as the t - J model may be interpreted to contain both retarded and non-retarded contributions.*

This is *qualitatively different in the 3BH-model*: Here, in Figs. 6 c) and f) and Fig. 8 b) we see a rather continuous “filling in” of integrated weight in the Ω regions in $I(\mathbf{k}, \Omega)$, where in the 1BH-model (Fig. 7 c)) this weight is clearly missing. This “filling in” is due to electron-hole excitations of $\mathcal{O}(2t_{pd})$ and, thus, due to p-d charge fluctuations (see the corresponding “red arrow” for the e - h transitions in $A(\mathbf{k}, \omega)$).

Thus, in the sense of the interpretations used for the 1BH-model above (and in Ref [30]) we may conclude that the *3BH-model is indeed different and contains only retarded contributions in its d-wave pairing interaction.*

In summary, then, the question posed in sect. III, i.e. whether there is a “pairing glue” in the 3BH-model is a question of whether the dominant contribution to the pairing function $\phi_1(\mathbf{k}, \omega = 0)$ comes from the integral of $\phi_2(k, \omega)/\omega$ and, more specifically, a “low-energy” (compared to $8t$) region in this integral. Earlier results have shown that both the 1BH- and t - J models exhibit spin-fluctuation “pairing glue” [30,31]. For both the 3BH-model as well as for the 1BH-model results, with the latter displayed for a similar higher-doping case (15%) in Fig. 7, one can include the full range of virtual e - h transitions between the lower and upper Hubbard bands. As a consequence the dispersion (Cauchy) relation for $\phi(\mathbf{k}, \omega = 0)$ does, strictly speaking, not contain a non-retarded contribution ϕ_{NR} and the asymptotic value of $I(\Omega)$ approaches unity. In the 1BH-model, we observe a first steep rise, which can again be identified with a typical spin-fluctuation energy. Then, at higher energies after a drop a second steep rise occurs at energies corresponding to (virtual) e - h interband transition of order $\sim \frac{U}{2}$. As argued in Ref. [30], it is this part which in the t - J model for $U \rightarrow \infty$ (i. e. when the upper Hubbard band is projected out) gives rise to an instantaneous contribution ϕ_{NR} . Thus, in this sense, both 1-band models also display a non-retarded interaction.

Our new result here is that *in the 3BH-model only low-energy (spin-fluctuation) retarded contributions to the pairing interaction dominate, whereas in the 1BH-model also a significant high-energy contribution occurs.* While these differences between a Mott and a charge-transfer insulator appear to be renormalized away in the very similar, i.e. “universal” ground-state phase diagram of these two models, one may use Eliashberg-type of arguments to form an expectation that the finite-T phase is rather different in the two models, i.e. strongly material-dependent (see also Ref. [27]).

V) Spin susceptibility

As is clear from the previous sections, two-particle (2-p) excitations, especially magnetic ones, are fundamental for understanding the issue of the “pairing glue” in high- T_c cuprate superconductors. In addition, for hole-doped cuprates in the superconducting (SC) state, the celebrated resonant magnetic mode emerges with its peak intensity being highest around the wave vector $Q_{AF} = (\pi, \pi)$ [45]. Away from Q_{AF} , the mode has both a downward and upward “hour-glass”-like dispersion. For electron-doped materials [46] the magnetic excitation spectrum has a different structure: it is confined to a small momentum region around (π, π) and it is essentially dispersionless [35].

In order to provide an appropriate description of the magnetic susceptibility and, in particular, of the magnetic resonance mode it is important to adopt a theory which is working in the experimentally relevant strong-correlation regime. As discussed above, VCA provides a suitable tool to study strongly-correlated systems for large lattices. In Ref. [34] we have developed a novel theory for two-particle excitations based on the VCA. This approach is, in contrast to previous weak-coupling and/or semiphenomenological treatments, parameter free and applies to the relevant strong-coupling regime of the one- and three-band Hubbard models. Within this method, two-particle susceptibilities are evaluated by first computing the *exact* two-particle irreducible vertex Γ within the reference system (cluster), and then inserting Γ into the Bethe-Salpeter (BS) equation for the exact (lattice) two-particle susceptibility [34]. Notice that the BS equation is in principle exact and not restricted to weak-coupling (in contrast to RPA). In principle, Γ depends on three frequencies and four cluster indices. Therefore, solving the BS equation with the corresponding full frequency and momentum dependence of Γ is a numerically quite expensive task. For this reason, we replace the full Γ with its average over external frequencies, and set the site indices pairwise equal, which corresponds to averaging over the external cluster momenta. After this simplification, $\Gamma(i\omega)$ can be computed as [34,47]

$$\Gamma(i\omega) = \left[(\chi^{0'}(i\omega))^{-1} - (\chi'(i\omega))^{-1} \right], \quad (11)$$

where χ' is the exact and $\chi^{0'}$ is the “bubble” susceptibility of the reference system, and ω is a Matsubara frequency. The term χ' in eq. (11) is evaluated directly within a Lanczos procedure and the first one is computed using the exact cluster Green’s functions. The effect of the above approximations is then partially compensated by multiplying $\Gamma(\mathbf{Q}, i\omega)$ by a constant term α which is determined so as to fulfill the sum rule for the transverse spin susceptibility. Details can be found in Ref. [34]. Finally, the lattice spin (or, corresponding charge) susceptibility, obtained by solving the BS equation, is given by

$$\chi(\mathbf{Q}, i\omega)^{-1} = \chi^0(\mathbf{Q}, i\omega)^{-1} - \alpha\Gamma(i\omega), \quad (12)$$

where $\chi^0(\mathbf{Q}, i\omega)^{-1}$ is the lattice “bubble” susceptibility evaluated with the fully dressed lattice Green’s functions. Since we are studying the superconducting phase, the bubble susceptibility has a contribution from both normal and anomalous Green’s functions. [34] Due to the partial breaking of translation symmetry introduced by the cluster tiling, both the χ_0 and χ depend on the wave vector \mathbf{Q} of the correspondingly reduced Brillouin zone, and are matrices in Nambu space as well as in the cluster sites.

In Ref. [25], as well as in the present paper, the qualitative similarity of the phase diagram and single-particle excitations between the three-band and the single-band Hubbard models was demonstrated. In particular, it was explicitly confirmed that the asymmetry between electron- and hole-doped cuprates, despite being of fundamentally different nature, shows very similar signatures in the single-particle spectrum of both models, provided a next-nearest-neighbor hopping t' , is included in the latter. The question remains whether this similarity can be extended to two-particle excitations. To address this question, we compare in Fig. 9 the imaginary parts of the spin susceptibility evaluated in the deeply underdoped regime ($x = 4\%$), for both the single- and the three-band models.

While there are some minor differences, both spectra display a dispersion which is a remnant of the spin-wave band in the antiferromagnetic half-filled phase. This fact signals the presence of strong antiferromagnetic fluctuations at this doping concentration also in a doped charge-transfer insulator.

Last not least, the *VCA-extension to 2-particle susceptibilities can account for* - without any adjustable parameters - *the magnetic resonance* in both hole- and electron-doping regimes. Close to optimal doping, the magnetic spectrum for the h-doped single-band Hubbard model (Fig. 10 a) shows the famous magnetic resonance peak at energies of about $0.1t - 0.2t$ and around wave-vector (π, π) . From this resonance, a downward dispersion extends down to the onset of the particle-hole continuum. The striking feature leading to the celebrated “hourglass” structure is, however, the additional “upward” dispersion, which can be seen in the spectrum of the single-band Hubbard model displayed in Fig. 10 a). Because of computational difficulties, we were not able to obtain this feature in the three-band model calculation. This is due to the fact that the smaller (2×2) CuO_2 -units cluster adopted for the three-band model still has significant antiferromagnetic correlations which prevent the formation of the hourglass structure (a similar observation holds also for the 1BH-model, where we had to go to (3×3) clusters (Fig. 10) to be able to observe the resonance).

In the electron-doped case, the magnetic excitation spectrum displays a different structure. In Fig. 10 b), we present the first strong-coupling and parameter-free evaluation of the magnetic spectrum in the

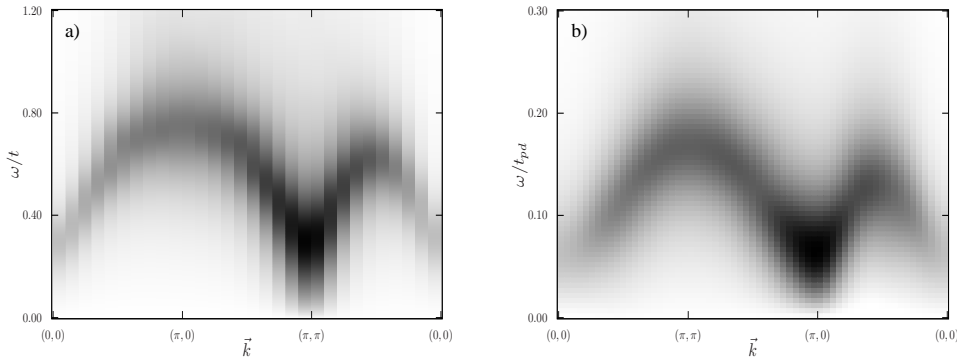


Figure 9. Imaginary part of the spin susceptibility $\chi''(\mathbf{k}, \omega)$ for the single-band (a) and for the three-band (b) Hubbard model at doping $x = 4\%$. Results are obtained with a reference system of (2×2) unit cells.

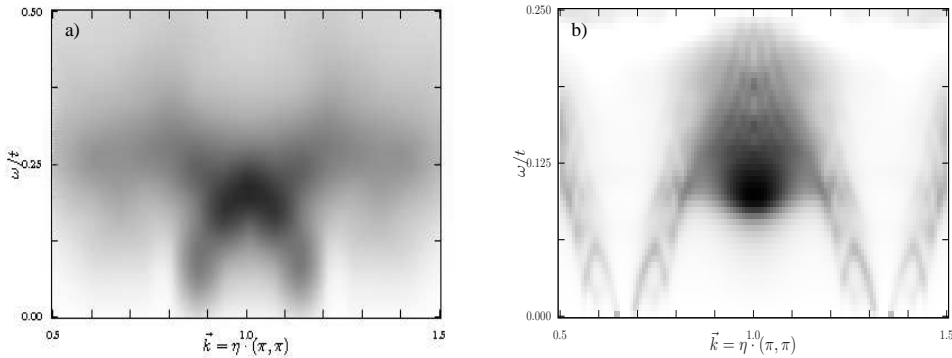


Figure 10. Imaginary part of the spin susceptibility for the single-band Hubbard model ((3×3) reference clusters, $U = 8t$) in the hole-doped ($x = 0.15$, a), taken from Ref. [34]) and in the electron-doped ($x = 0.14$, b) cases.

electron-doped case, within our VCA approach for two-particle excitations. As one can see, in this case the weight of the magnetic spectrum is concentrated essentially in the vicinity of (π, π) , in accordance with the experimental situation. The downward dispersion observed in the calculation only carries very little weight, when compared with the strong peak around (π, π) . Therefore, this might be the reason why this dispersion is not seen in inelastic neutron scattering experiments [46]. Finally, in contrast to the hole-doped case, the upward dispersion is not observed for electron doping. This is also in accordance with the experimental observations [35].

We have also extended, in a similar spirit, the dynamical cluster approximation (DCA) to 2-p susceptibility calculations at finite-temperatures [47] for the infinite-lattice case. In Ref. [47], this scheme has been used to obtain - in the case of the 1BH-model - information on the finite-T phase diagram (via the instability towards a symmetry-broken phase of the corresponding susceptibility).

VI) Conclusion

One key issue in the research on high- T_c cuprate superconductivity is to derive a detailed understanding for the specific role of the $Cu-d_{x^2-y^2}$ and $O-p_{x,y}$ orbital degrees of freedom. Very early on a corresponding three-band Hubbard (3BH) model has been suggested but in most studies an effective one-band Hubbard (1BH) or t - J model has been used. The one-band models have been shown, using a variety of techniques, to reproduce salient features of the cuprates such as the competing antiferromagnetic (AF) and superconducting (SC) phases including the electron-versus-hole doping asymmetries. Here, the physics is that of doping into a Mott-Hubbard insulator, whereas the actual high- T_c cuprates are doped charge-transfer

insulators. Using a cluster embedding scheme, i.e. the variational cluster approach (VCA) which allows for a controlled route to go to the large system size limit (and, thereby, low-energy limit), we compare in detail the competing phases in the ground-state, the single-particle and two-particle excitations and, in particular, the dynamic pairing interaction and the issue of a “pairing glue” of the 3BH and 1BH model. This study demonstrates that there are pronounced differences on a “higher-energy” scale (compared to the SC gap energy) for the two models, such as the charge-transfer energy Δ_{pd} in the 3BH-model. While these “high-energy” features, where the material-dependent physics enters, play no decisive role for the overall structure of the phase diagram, which shows excellent agreement between 3BH- and 1BH-models, there appear significant differences in the dynamics of the pairing interaction: in the 3BH-model the interaction is dominated by a retarded pairing due to low-energy spin fluctuations, whereas in the 1BH-model in addition a part comes from excited states involving the upper Hubbard band, which may be associated with a “non-retarded” contribution. Thus, one may term the ground-state phase diagram “universal”, whereas the different dynamics of the pairing interaction of the two models should be reflected in a pronounced material dependence of the finite-T phase diagram.

First steps in this direction have already been undertaken in Ref. [27] and are also presently followed up in our group [48].

Finally a comment about the RVB-type of physics in the two models: Δ_{pd} also enters in the exchange coupling J between spins on the Cu sites. Thus, the role of U in the 1-band model, setting the characteristic energy of the RVB-coupling J , is taken over (see Eq. (9)) in the 3-band model by the energy of the $p-d$ charge fluctuations. In that sense, one may argue, that the final increase in the relative pairing strength $I(\mathbf{k}, \omega)$ to the value of $I(\mathbf{k}, \omega) = 1$ again reflects RVB physics. However, our results demonstrate that there is quite a difference with respect to the relative weights of the spin-fluctuation and higher-energy contributions between the two models.

Acknowledgments

We acknowledge detailed discussions with D.J. Scalapino, Th. Maier and M. Potthoff and financial support from the DFG HA1537/21-3, from the Bavarian supercomputer network KONWIHR and from the FWF P18551-N16.

References

1. J. Zaanen, G. A. Sawatzky and J. W. Allen, Phys. Rev. Lett. **55**, 418 (1985)
2. V. J. Emery, Phys. Rev. Lett. **58**, 2794 (1987), V. J. Emery and G. Reiter, Phys. Rev. B **38**, 4547 (1988), and C. M. Varma and S. Schmitt-Rink, Sol. St. Comm. **62**, 681 (1987)
3. F. C. Zhang and T. M. Rice, Phys. Rev. B **37**, 3759 (1988), **41**, 7243 (1990)
4. G. Dopf, A. Muramatsu and W. Hanke, Phys. Rev. B **41**, 9264 (1990)
5. G. Dopf, A. Muramatsu and W. Hanke, Phys. Rev. Lett. **68**, 353 (1992)
6. P. Horsch, W. H. Stephan, K. v. Szczepanski, M. Ziegler and W. von der Linden, Physica C **162-164**, 783 (1989)
7. R. T. Scalettar, D. J. Scalapino, R. L. Sugar and S. R. White, Phys. Rev. B **44**, 770 (1991)
8. P. Unger and P. Fulde, Phys. Rev. B **48**, 16607 (1993)
9. A. Macridin, M. Jarrell, Th. Maier and G. A. Sawatzky, Phys. Rev. B **71**, 134527 (2005)
10. For recent work see: L. de Medici, X. Wang, M. Capone and A. J. Millis, Phys. Rev. B **80**, 054501 (2009) and C. Weber, K. Haule and G. Kotliar, Phys. Rev. B **78**, 134519 (2008)
11. P. W. Anderson, Science **235**, 1196 (1987)
12. For a review see: M. Imada, A. Fujimori and Y. Tokura, Rev. Mod. Phys. **70**, 1039 (1998) and Refs. therein.
13. R. Preuss, C. Gröber, H. G. Evertz and W. Hanke, Phys. Rev. Lett. **79**, 1122 (1997)
14. D. D. Sènèchal, P.-L. Lavertu, M.-A. Marois and A.-M. S. Tremblay, Phys. Rev. Lett. **94**, 156404 (2005)
15. T. A. Maier, M. Jarrell, T. C. Schulthess, P. R. C. Kent and J. B. White, Phys. Rev. Lett. **95**, 237001 (2005)
16. M. Aichhorn, E. Arrigoni, M. Potthoff and W. Hanke, Phys. Rev. B **74**, 024508 (2006)
17. M. Aichhorn, E. Arrigoni, Z. B. Huang and W. Hanke, Phys. Rev. Lett. **99**, 257002 (2007)
18. A. Macridin, M. Jarrell, T. Maier, P. R. C. Kent and E. D’Azevedo, Phys. Rev. Lett. **97**, 036401 (2006)

19. T. A. Maier, M. Jarrell and D. J. Scalapino, Phys. Rev. B 76, 144516 (2007); *ibid.* 75, 134519 (2007)
20. D. J. Scalapino, Chapter 13 in the “Handbook of High Temperature Superconductivity”, J. R. Schrieffer (editor), Springer (2006)
21. P. A. Lee, N. Nagaosa and X.G. Wen, Rev. Mod. Phys. 78, 17, (2006)
22. F. Assaad, W. Hanke and D. J. Scalapino, Phys. Rev. Lett. 71, 1915 (1993) and Phys. Rev. B 50, 12835 (1994)
23. M. Potthoff, Eur. Phys. J. B 32, 429 (2003)
24. C. Dahnken, M. Aichhorn, W. Hanke, E. Arrigoni and M. Potthoff, Phys. Rev. B 70, 245110 (2004)
25. E. Arrigoni, M. Aichhorn, M. Daghofer and W. Hanke, New. J. Phys. 11, 055066 (2009)
26. H. Eskes, G. A. Sawatzky and L. Feiner, Physica C 160, 424 (1989)
27. P. R. C. Kent, T. Saha-Dasgupta, O. Jepsen, O. K. Andersen, A. Macridin, T. A. Maier, M. Jarrell, T. C. Schulthess, Physical Review B 78, 035132 (2008)
28. M. Aichhorn, W. Hanke, Phys. Rev. B 74, 235117 (2006)
29. P. W. Anderson, Science Vol. 317, 1705 (2007)
30. T. A. Maier, D. Poilblanc and D. J. Scalapino, Phys. Rev. Lett. 100, 237001 (2008)
31. B. Kyung, D. Sènèchal and A.-M. S. Tremblay, Phys. Rev. B 80, 205109 (2009)
32. M. Civelli, Phys. Rev. Lett. 103, 136402 (2009)
33. T. Valla, T. E. Kidd, W.-G. Yin, G. D. Gu, P. D. Johnson, Z.-H. Pan and A. V. Fedorov, Phys. Rev. Lett. 98, 167003 (2007) and D. S. Inosov, J. Fink, A. A. Kordyuk, S. V. Borisenko, V. B. Zabolotnyy, R. Schuster, M. Knupfer, B. Büchner, R. Follath, H. A. Dürr, W. Eberhardt, V. Hinkov, B. Keimer and H. Berger, Phys. Rev. Lett. 99, 237002 (2007)
34. S. Brehm, E. Arrigoni, M. Aichhorn and W. Hanke, Europhys. Lett. 89, 27005 (2010)
35. J.-P. Ismer, I. Eremin, E. Rossi and D. K. Morr, Phys. Rev. Lett. 99, 047005 (2007) and I. Eremin, D. K. Morr A. V. Chubukov, K. H. Bennemann and M. R. Norman, Phys. Rev. Lett. 94, 147001 (2005)
36. A. Abanov and A. V. Chubukov, Phys. Rev. Lett. 83, 1652 (1999); I. Sega, P. Prelovšek, and J. Bonča, Phys. Rev. B 68, 054524 (2003); P. Prelovšek and I. Sega, Phys. Rev. B 74, 214501 (2006), R. Zeyher Europhys. Lett. 90, 17006 (2010)
37. E. Demler, W. Hanke and S. C. Zhang, Rev. Mod. Phys. 76, 909 (2004)
38. L. P. Pitaevskii, Sov. Phys. JETP 10, 1267 (1960)
39. K. A. Bruechner, T. Soda, P. W. Anderson and P. Morel, Phys. Rev. 118, 1442 (1960)
40. L. N. Cooper, Phys. Rev. 104, 1189 (1956)
41. P. Morel and P. W. Anderson, Phys. Rev. 125, 1263 (1952)
42. G. M. Eliashberg, Soviet Phys - JETP II, 696 (1960)
43. D. J. Scalapino, Physics Reports 250, 329365 (1995) and in Random Magnetism, High-Temperature Superconductivity, W. P. Beyermann et. al., eds. (World Scientific, Singapore, 1994, p. 155-164)
44. G. Dopf, A. Muramatsu and W. Hanke, Phys. Rev. B 41, 9264 (1990)
45. S. Pailhes, Y. Sidis, P. Bourges, V. Hinkov, A. Ivanov, C. Ulrich, L. P. Regnault and B. Keimer, Phys. Rev. Lett. 93, 167001 (2004)
46. S. D. Wilson, P. Dai, S. Li, S. Chi, H. J. Kang and J. W. Lynn, Nature London 442, 59 (2006)
47. S. Hochkeppel, F. Assaad, W. Hanke, Phys. Rev. B 77, 205103 (2008)
48. G. Li, Th. Maier, E. Arrigoni and W. Hanke (unpublished)
49. T. Dahm, V. Hinkov, S.V. Borisenko, A.A. Kordyuk, V.B. Zabolotnyy, J. Fink, B. Büchner, D.J. Scalapino, W. Hanke, B. Keimer, Nature Physics 5, 217-221 (18 January 2009)